

pubs.acs.org/acsaelm Article

Shadow Wall Epitaxy of Compound Semiconductors toward All in Situ Fabrication of Quantum Devices

Nils von den Driesch,* Yurii Kutovyi, Felix Khamphasithivong, Anja Zass, Lars R. Schreiber, and Alexander Pawlis



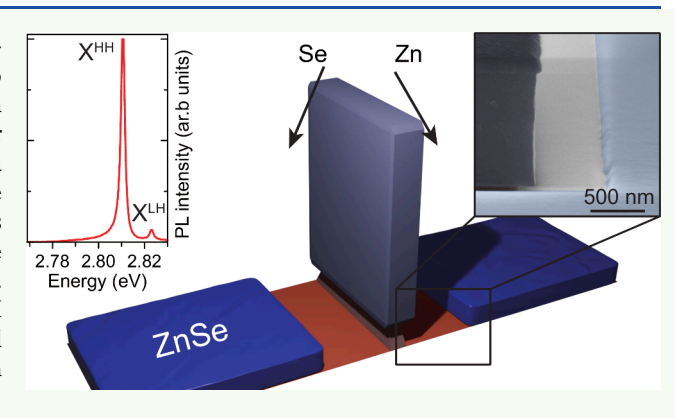
Cite This: ACS Appl. Electron. Mater. 2024, 6, 6246-6252



ACCESS |

III Metrics & More

ABSTRACT: The realization of advanced semiconductor nanostructures requires the development of epitaxial growth schemes to mitigate the detrimental effects of ex situ device processing. With this perspective, we introduce a selective growth concept for molecular beam epitaxy (MBE) in which parts of the sample area are shadowed using prefabricated walls. Systematic analysis of the crystalline and optical properties by X-ray diffraction techniques and photoluminescence reveal a comparably good quality of the structured ZnSe-based thin films, compared to reference samples. We transfer this concept toward epitaxy of more complex II-VI heterostructures to demonstrate the versatility of our epitaxial approach for the development of fully in situ processed quantum devices.



Article Recommendations

KEYWORDS: MBE, selective area growth, epitaxy, compound semiconductors, ZnSe

INTRODUCTION

Compound semiconductors made from II-VI materials are a well-known platform for optical applications in the full visible spectrum. 1-4 Their natural material properties make them especially appealing for novel photonic components in quantum information technology. In ZnSe, for example, efficient radiative recombination from the direct bandgap of 2.8 eV allows for the synthesis of single-photon sources and facilitates straightforward developments toward spin-photon interfaces.^{9,10} Furthermore, the possibility for isotopically purifying the nuclear spin toward zero in these materials¹¹ enables the achievement of extended spin decoherence times. 12

Considering that the formation of local, low-ohmic electrical contacts at cryogenic temperatures (down to 4 K) was demonstrated on n-ZnSe, 13 this could be used to realize prospective all-electrical quantum devices, such as electrostatically defined spin qubits in semiconductors, 14-17 without the issue of lifting the valley degeneracy from which the frontrunner Si/SiGe suffers. 18-20 However, the demonstrated approaches require additional ex situ fabrication steps in between, such as dopant implantation, electron-beam lithography and reactive-ion etching. The necessary relieving of the ultrahigh vacuum carries the additional danger of surface oxidation, which introduces many defects and degrades the inherent device properties, such as carrier mobility and electrostatic disorder. These drawbacks can be circumvented during MBE growth, which remains one of the most important

techniques for manufacturing selenide-based materials today. 21-23 Here, the introduction of selective area growth schemes can facilitate in situ definition of spatially localized device and contact areas already during epitaxy. 24,25 Traditionally, the strong diffusion dynamics during III-V material growth easily allows for the growth of self-assembled nanostructures such as InAs quantum dots or wires.^{26,27} The much weaker ordering effects during II-VI epitaxy,28 however, require the use of shadow masks that restrict epitaxial growth only within well-defined cavities.^{29,30}

Alternatively, a novel selective growth concept for MBE is introduced in this contribution, which enables material deposition on large parts of the sample, while only small regions are shadowed. Our approach is based upon prefabricated walls on top of GaAs wafers, which shadow neighboring sample regions at will by changing the sample orientation in regard to the material flux. Similar approaches using shadow walls were used in literature before, but so far only for deposition of elemental superconductors and metals.31,32 In the following, we will demonstrate the

Received: June 21, 2024 Revised: August 9, 2024 Accepted: August 12, 2024 Published: August 19, 2024





shadowing effect during growth of compound semiconductor materials and discuss a possible influence on crystalline and optical quality of as-grown ZnSe thin films and ZnSe/ZnMgSe quantum well (QW) heterostructures.

EXPERIMENTAL SECTION

In this work, II—VI thin films were grown using MBE on GaAs substrates, prepatterned with shadow wall structures. The process flow for the shadow wall fabrication is schematically shown in Figure 1(a)-(d). First, the material stack consisting of 100 nm of SiO_2 and

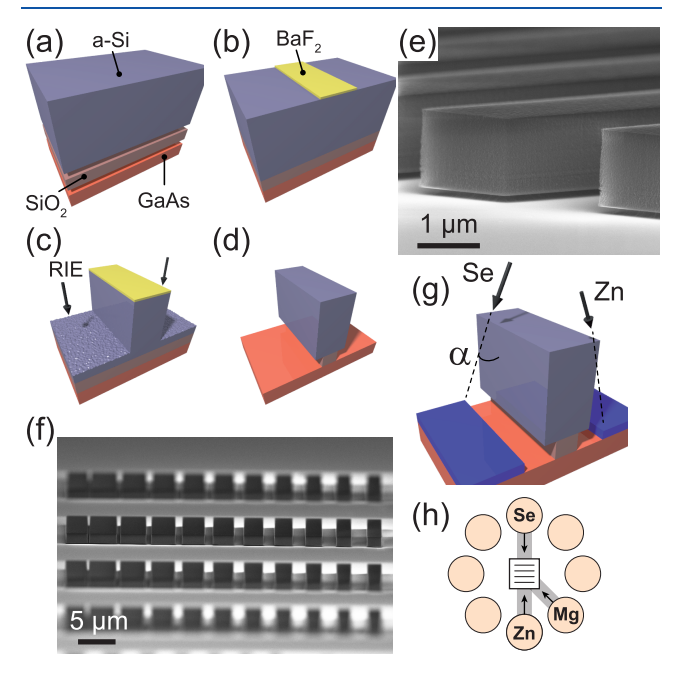


Figure 1. (a)-(d) Fabrication process of the proposed shadow walls and (e),(f) SEM micrographs of finished shadow wall structures. (g) Schematic shadowing principle of the produced walls, using the MBE's effusion cell arrangement depicted in (h).

1200 nm of amorphous Si is e-beam evaporated on epi-ready undoped GaAs (001) substrates (see Figure 1(a). Electron beam lithography is then performed to predefine the shadow wall structures in a positive tone AR-P 6200 resist. In the next step, a 100 nm thick BaF2 layer is evaporated onto the substrates and patterned using a lift-off process, as shown in Figure 1(b). Afterward, the top Si layer is dry-etched by $SF_6/Ar/CH_4$ plasma employing reactive-ion etching technique, using the BaF2 pattern as an etch hard mask (see Figure 1(c). Finally, a short time wet-chemical etch with hydrofluoric acid (1%) is performed to ensure removal of both the water-soluble BaF2 hard mask and the SiO2 layer, which therefore exposes a pristine GaAs surface, as depicted in Figure 1(d). Typical scanning electron microscopy (SEM) micrographs of shadow wall structures after fabrication are presented in Figure 1(e) and (f), showing nearly structures

After loading the prestructured samples into the ultrahigh vacuum (UHV) system and prior to the actual epitaxy, the samples are exposed to an atomic hydrogen cleaning step to ensure removal of possible carbon compounds from the previous cleanroom processing. Then, samples are transferred to a dedicated III—V chamber for oxide desorption and growth of a 100 nm thick GaAs buffer layer. In some samples, the GaAs buffer growth step was performed prior shadow wall fabrication and the previously described atomic hydrogen step was used for sample deoxidation, ³³ see Table 1 for details. For epitaxy of the II—VI compounds, the samples are transported to a second dedicated MBE chamber using a UHV transfer line, which ensures a pristine sample surface for growth start. Material fluxes from

Table 1. Overview of the Grown Sample Structures

Sample	Structure	GaAs buffer	Shadow mask	ZnSe/ ZnMgSe thickness (nm)	Mg concentration (%)
A	ZnSe	Prior fabrication	Yes	100	-
В	ZnSe	Yes	Yes	63	-
C	ZnSe	Yes	No	42	-
D	ZnSe/ ZnMgSe QW	Yes	Yes	9/29	-/19

elemental zinc and magnesium effusion cells were used with beam equivalent pressures reading values of roughly 3×10^{-7} mbar and 2×10^{-8} mbar, respectively. A valved selenium cracker cell with an additional linear shutter is used for supply of the molecular Se beam. It allows quick ramping of the Se flux and delivers a beam equivalent pressure reading of approximately 2×10^{-6} mbar during ZnSe growth. The growth is performed at a nominal substrate temperature of 290 °C under Se-rich conditions. In order to achieve an abrupt and epitaxially perfect III–V/II-VI interface, excess Zn was supplied during growth of the first few nm of the ZnSe buffer layer.

RESULTS AND DISCUSSION

Our selective shadow mask growth scheme relies on the relative orientation of the sample and its shadow walls toward the incident molecular beams, as schematically depicted in Figure 1(g). For this, metal and nonmetal effusion cells are arranged in a circular shape and on opposite sides of the sample in our MBE system, shown in Figure 1(h). Therefore, rotating the sample to a position, in which the shadow walls are aligned perpendicular toward those material fluxes will suppress epitaxial growth directly adjacent to a wall. This is due to the sticking coefficients of elemental Zn and Se being practically zero at growth temperatures in absence of their compound partner.³⁴ In the following, we assign this growth configuration as "shadow alignment" (ShA). Given a wall height of 1.3 μ m and a relative tilt α of the material sources (see Figure 1(g)) of 30°, we aim for geometrical shadow regions of roughly 700 nm width using our approach. It should also be noted that the height of the wall can be chosen significantly higher, which leads to correspondingly larger shadow regions as well. Accordingly, shorter walls will result in smaller shadow regions, allowing the formation of nanosized areas for quantum devices. In the second possible configuration, the sample is rotated by 90°. Here, the shadow walls are aligned parallel toward the material flux, so growth will take place even directly next to the wall. This geometry is termed as "nonshadow alignment" (NShA).

Two different types of structures, ZnSe thin films and a ZnSe/ZnMgSe quantum well (QW), were subsequently grown on top of various structured samples. For quality assessment, an additional reference ZnSe sample was grown on a pristine GaAs(001) wafer without shadow walls. Further structural details on the as-grown structures can be found in Table 1.

A top view SEM micrograph of a 100 nm ZnSe thin film, grown on a shadow wall-structured sample (Sample A), is shown in Figure 2(a). For this sample, the GaAs buffer growth was performed prior wall fabrication to allow a distinct assignment of the resulting shadows of the ZnSe process. The incident Zn and Se fluxes were aligned along the depicted cross, resulting in suppression of material growth in regions, in which one of the material fluxes is shadowed. This is even more evident in the 85° tilted SEM micrograph displayed in

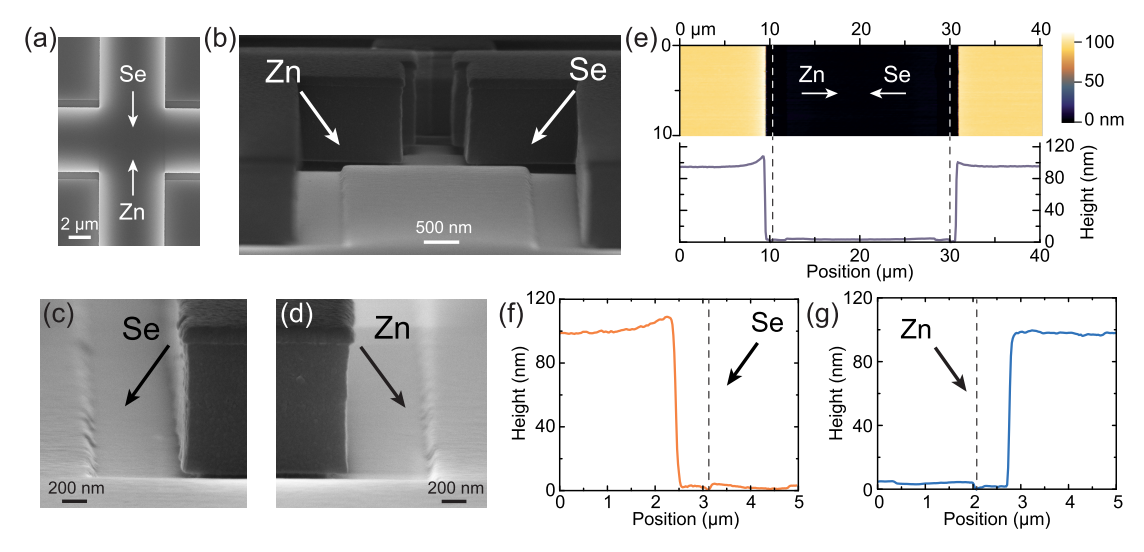


Figure 2. Demonstration of shadow effect during ZnSe growth in (a) top and (b) tilted view SEM micrographs. Tilted SEM micrographs of the (c) Se shadow and the (d) Zn shadow region. (e) AFM micrograph and linescan showing large areas of ZnSe growth and shadow regions after *ex situ* wall removal. The former wall positions are indicated by dotted lines. AFM linescans through the (f) Se shadow and (g) Zn shadow region.

Figure 2(b), where the directions of Zn and Se fluxes are indicated by arrows. ZnSe was grown only in the middle region between the walls, where both material fluxes overlap. In areas directly neighboring one of the walls, epitaxy is strongly suppressed. Accordingly, if the shadow wall spacing is smaller than the shadow length of roughly 700 nm, epitaxy is also suppressed, as visible in the background of said micrograph. Regions of Se and Zn shadows are shown at higher magnification in Figure 2(c) and (d), respectively. In here, the transition between fully shadowed and unaffected areas is visible, indicated by nonvertical side facets of the grown ZnSe thin film.

Atomic force microscopy (AFM) measurements in these shadow edge regions were performed to gain microscopic understanding on the shadow formation and possible limitations of our growth method. Figure 2(e) shows an AFM micrograph and linescan across both Zn and Se shadow regions. The shadow wall was chemically removed prior measurement using hydrofluoric acid (1%), its former position is indicated by dashed lines. Furthermore, the directions of Zn and Se fluxes are indicated by arrows. The AFM micrograph shows straight shadow edges along several μ m, underlining the high quality of the fabricated shadow walls. A linescan across the whole region again clearly shows shadowed regions adjacent to the former walls. A closer view into the Se shadow region is shown in Figure 2(f), proving no material growth directly adjacent to the wall (former position marked by dashed lines). The broadening of the shadow edge, given by the step width, can be determined to a value of 120(10) nm. Typically, diffusion dynamics should not limit the formation of steep edges in ZnSe selective growth down to a few tens of nm,³⁵ therefore, we attribute the broadening to a combination of several factors. For one thing, a partial shadow width of roughly 100-150 nm can be expected from a simple calculation considering the finite cell orifice, shadow wall height and distance between sample and evaporation cells. This value could be easily reduced using apertures in front of the evaporation cells. Second, material growth on top of the walls (visible also in the micrographs in Figure 2(c) and (d)) can broaden the shadow edge additionally during growth. An additional feature, observed in Figure 2(f), is a distinct

overshoot of the local ZnSe growth rate close to the transition region. Since growth is performed under Se-rich conditions, a secondary Zn flux, e.g. reflected from the shadow wall, will locally increase the ZnSe growth rate. Accordingly, this increase is much less pronounced in the Zn shadow region shown in Figure 2(g), where the possible increase in Se flux due to reflection from the wall does not have any impact on the local growth rate.

To demonstrate a high material quality despite the preepitaxial cleanroom processing, two ZnSe thin film samples B and C were grown, of which only the former featured shadow walls. Structural analysis of both layers is shown in Figure 3. In (a), specular ω -2 θ scans of the (004) reflexes of samples B and C are presented. Peaks from both the GaAs substrate (at 66.08°) and the ZnSe thin film (at 65.63°) can be well distinguished. Typical thickness fringes of pseudomorphically grown layers are clearly visible, indicating atomically smooth interfaces without any defect-induced strain relaxation. The different periodicity of those fringes is due to slightly different layer thicknesses of 63 nm (B) and 42 nm (C), however, both values are well below the critical thickness for strain relaxation of ZnSe on GaAs.³⁶ The inset of Figure 3(a) displays rocking curves (ω scans) around the ZnSe (004) reflexes. In those, samples B and C exhibit comparable fwhm values of 59" and 53", respectively, which confirms the successful pre-epi treatment using atomic hydrogen.

In Figure 3 (b) a distinct impact of the procedure on the surface morphology is visible. Here, $2 \times 2 \mu m$ AFM micrographs of samples B and C show clear differences in surface roughness. For the case of the reference ZnSe thin film sample C, a very smooth surface is found, underlined by a small root-mean-square (rms) roughness of 0.2 nm. For the shadow wall-structured sample B, however, we observed a distinctly higher rms roughness value of 1.0 nm, indicating that the pre-epi surface cleaning procedure may still be improved. It shall be noted that part of the observed difference of the samples' surfaces may be explained by the onset of an unavoidable selenium oxide cluster formation in sample B, since an exposure of the sample to ambient conditions of one hour occurred prior AFM scanning. 37

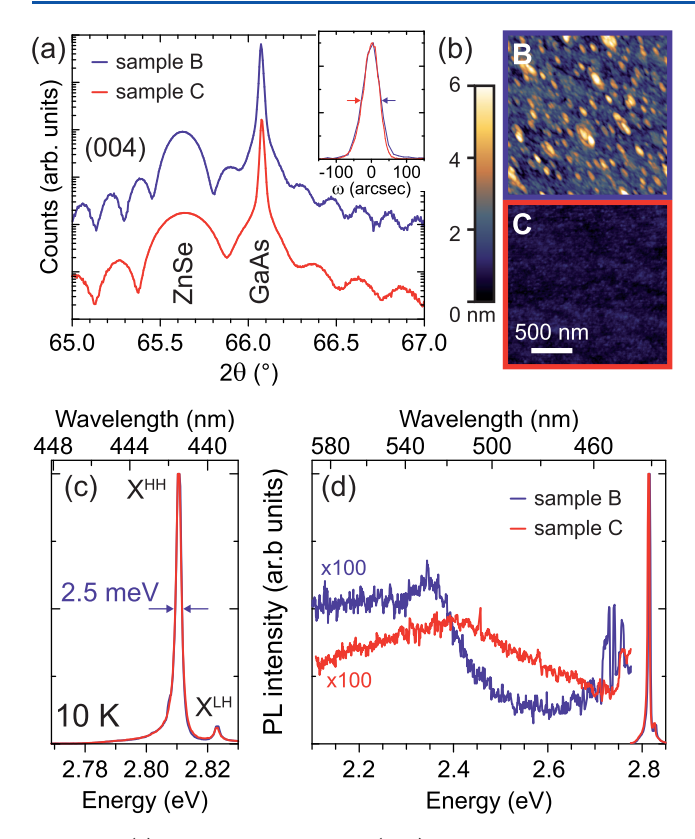


Figure 3. (a) ω -2 θ scan around the (004) reflexes of a shadow wall-grown (B) and reference ZnSe sample (C), with ω scans across the ZnSe (004) reflexes as inset. (b) 2 × 2 μ m AFM micrographs from samples B and C. (c), (d) Photoluminescence spectra of both samples covering the excitonic and the near-bandgap spectral regions, respectively.

Next, the layers' optical properties are compared to obtain a more precise knowledge about possibly involved impurities which, even at low density, are revealed by low temperature photoluminescence (PL) measurements. Figure 3(c) depicts the excitonic emission region of both samples, demonstrating

virtually no difference in PL signal. The typical free-exciton transition in both samples is split by the present compressive strain into two transitions $X^{\rm HH}$ and $X^{\rm LH}$, involving holes from the heavy and light hole subbands. The fwhm line width of the X^{HH} transition is determined to 2.5 meV at a pumping power of 1 μ W. Apart from those two transitions, however, neither additional donor- nor acceptor-bound excitons with binding energies up to 40 meV are observed on the lower energy side. A broader spectral range of the PL is shown in Figure 3(d). For an easier comparison of both spectra, the parts below 2.75 eV are multiplied by a factor of 100. While no pronounced impurity-related peaks are visible in reference C, a small number of defect-related transitions appear in sample B below the energy of 2.74 eV. The multitude of peaks is typically assigned to donor-acceptor-pair (DAP) transitions and their phonon replicas.³⁸ The absence of PL emission from single impurity-bound exciton complexes (D⁰X or A⁰X) suggests that the remaining shallow impurity concentration is negligible small and compensated. Additionally, a rather broad PL region between 2.1 and 2.5 eV is present in both samples, often assigned to defect complexes involving V_{Zn}.

For demonstration of the versatility of our shadow wall approach, a complete ZnSe/ZnMgSe QW heterostructure was grown. During growth, the sample was rotated in a way, which ensured a ShA orientation during ZnSe QW layer growth, while the ZnMgSe barrier layers were grown in the NShA orientation. For this sample, roughly 5 μ m tall shadow walls consisting purely of SiO₂ were employed, leading to a theoretical shadow length of roughly 3 μ m. A sketch of the resulting layer structure can be found in Figure 4(a), where a ZnSe QW is formed far away from any structures. Since QW growth is suppressed directly adjacent to the shadow walls, only a ZnMgSe film from the barriers is expected to be present there. Figure 4(b) shows an XRD reciprocal space map (RSM) around the (224) reflexes, recorded far away from the shadow regions. The ZnSe/ZnMgSe heterostructure is only slightly strain-relaxed on top of the GaAs substrate (\sim 3%), indicated by the nearly matching in-plane lattice constants apar. In conjunction with symmetric (004) ω -2 θ scans (not shown

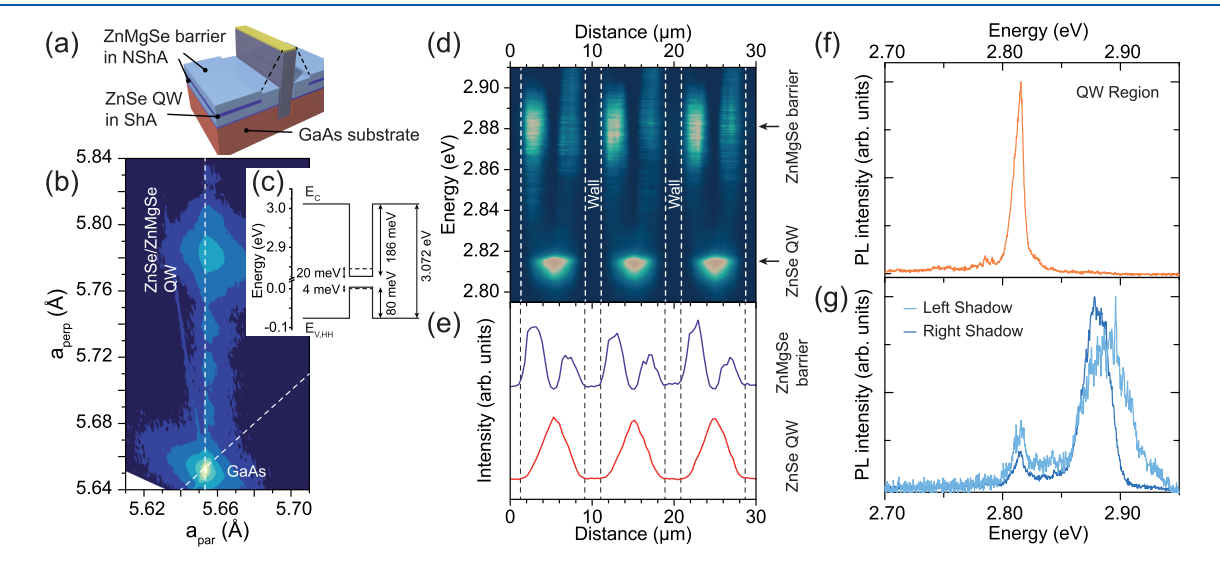


Figure 4. (a) Sketch of the epitaxially grown ZnSe QW structure under influence of shadow walls. (b) Reciprocal space map surrounding the (224) reflexes confirm a coherently grown ZnSe QW. (c) Calculated band alignment of the grown QW structure. (d) PL mapping across the shadow wall structures and (e) spatially resolved constant energy lines of ZnSe QW and ZnMgSe barrier PL. (f) and (g) PL spectra of the QW and shadowed regions, respectively.

here), a ZnSe well thickness of 9 nm is determined, while the 28 nm thick ZnMgSe barriers have a Mg concentration of 19%.

We calculated the band diagram of the grown ZnSe/ ZnMgSe QW using a finite barrier model and the experimentally determined composition, biaxial strain and layer thickness. The parameters for ZnSe and MgSe, i.e. effective masses, bandgaps, elastic and lattice constants and deformation potentials, are listed in reference.³⁹ For the ZnMgSe barriers, a linear interpolation of those parameters, depending on the composition, was employed. The corresponding band diagram at the Gamma point is shown in Figure 4(c) for conduction and heavy hole valence band. The confinement for electrons and heavy holes in the quantum well is defined by the band offsets of 186 and 80 meV, respectively. These values, resulting from the rather high Mg concentration in the barrier, are well above the thermal energy at 10 K. Therefore, it is more than sufficient to localize carriers and excitons inside the QW region, given also the rather small quantization in the 9 nm thin well, shown in Figure 4(c) as well. The strong localization is preserved even up to elevated temperatures and allows the formation of a 2D electron gas, making devices from such structure ideal candidates for electrostatically defined spin qubits.

Photoluminescence (PL) linescans across an array of shadow walls at 5 K are used to probe the optical properties of the sample and to verify the shadowing effect. For this purpose, a micro-PL setup with an excitation spot size of approximately 1 μ m was used. Three separated PL regimes are visible in the PL linescan spectra in Figure 4(d). The region of the SiO₂ shadow walls is easily identified from the missing PL signal and labeled correspondingly. In the intermediate nonshadowed region between these walls, approximately 3 μ m wide, a strong PL signal at around 2.815 eV can be attributed to emission from the ZnSe QW. The slightly higher emission energy compared to that in both previous ZnSe samples B and C (c.f. Figure 3(c) can be ascribed to the effect of quantum confinement in the QW. A PL spectrum from the QW region is shown in Figure 4(f), underlining the absence of any pronounced defect-related emission peak.

Two additional PL regions are visible neighboring the shadow walls in the PL map of Figure 4(d). Here, PL emission is seen only at distinctly higher energies of approximately 2.89 eV. This value is well above the ZnSe bandgap and must, therefore, originate from the ZnMgSe barrier layers. Photoluminescence spectra from that region, visible in Figure 4(g), show a dominance of the broader, larger bandgap ZnMgSe emission. In conjunction with the strong suppression of the QW emission in these regions, likely only visible due to the finite excitation spot size or diffusion of photoexcited carriers, this is unambiguous prove of the proposed shadowing effect in the grown configuration.

Yet, there is a slight asymmetry between both shadow regions (i.e., left- and right-hand sides of the wall), which is also pronounced in linescans at constant energies shown in Figure 4(e). In the left-hand shadow side of the walls, the PL shows a consistently smaller intensity, which we attribute to the cell geometry of our MBE chamber. Since Zn and Mg cells cannot be aligned parallel (c.f. Figure 1(h)), Mg atoms impinge the shadow wall rotated by about roughly 45°. Their reflection from the wall can locally increase the growth rate and Mg incorporation on the Se shadow side, similar as we observed from our AFM studies in Figure 2(f). The higher Mg concentration would deteriorate the local crystal quality and,

thus, also affect the PL emission. This explanation is underlined by the fact that a visible shift of the peak of the ZnMgSe PL emission to higher energies can be observed for the case of the left-hand shadow region in Figure 4(g). This shift of roughly 8 meV can be converted into a 0.6 percentage point increase in Mg concentration on that side of the wall using a simple Vegard's law calculation.³⁹ It should be noted at this point, however, that the observed asymmetry only influences the barriers in the shadow regions. The ZnSe QW region in between the walls is completely unaffected by this.

The width of the formed QW region in above structure is solely defined by the height and distance of the shadow walls and is approximately 3 μ m. Therefore, using appropriate shadow wall designs, in situ formation of nanostructured areas during epitaxy for active devices is possible. For example, a simple reduction in wall spacing leads to QW regions with less than 100 nm widths and, therefore, to the local formation of quasi-1D nanowires.

Using special shadow wall designs and orientations during growth, the *in situ* formation of complete electronic devices may also become possible. If, for example, in the considered design above (Figure 4(a)) the upper barrier was also shadowed (in addition to the quantum well) close to the wall, only the bottom ZnMgSe barrier will be grown in that part. In case of a grown ZnSe diode structure, this open window may allow a direct and etch-free, *in situ* metallization of the buried bottom contact. In the field of optoelectronics, this may result in improved device characteristics of light emitting diodes and lasers compared to conventional *ex situ* processing.

CONCLUSION

In this work, we investigated a novel selective epitaxial growth concept using Si/SiO2-based shadow walls. We demonstrated an unambiguous shadowing effect during II-VI semiconductor deposition, which enables in situ structuring of MBE thin films. Despite the pre-epitaxial shadow mask fabrication, the resulting films show a consistently high crystalline quality compared to reference samples, as determined by XRD measurements. Furthermore, PL spectra from the near bandgap region indicate no increased number of shallow or deep-level defects and, thus, a comparable optical quality as well. Finally, we applied our shadow wall concept to demonstrate laterally controlled deposition of semiconductor heterostructures. Different material regions, namely with and without ZnSe QWs, have been defined in situ and verified by means of spatially resolved PL. Although we focus on the growth of II-VI compounds in this publication, many other material systems, such as metals or oxides, can be integrated into our approach as well. Ultimately, this opens up a whole range of complex nanostructures, which can be grown under ultrahigh vacuum conditions and tailored for different applications within quantum information technology.

AUTHOR INFORMATION

Corresponding Author

Nils von den Driesch – Peter Grünberg Institute 10 (PGI 10), Forschungszentrum Jülich, 52428 Jülich, Germany; JARA-Fundamentals of Future Information Technology (JARA-FIT), 52428 Jülich, Germany; orcid.org/0000-0003-0169-6110; Email: n.von.den.driesch@fz-juelich.de

Authors

- Yurii Kutovyi Peter Grünberg Institute 9 (PGI 9), Forschungszentrum Jülich, 52428 Jülich, Germany; JARA-Fundamentals of Future Information Technology (JARA-FIT), 52428 Jülich, Germany; orcid.org/0000-0002-3905-2575
- Felix Khamphasithivong JARA-FIT Institute for Quantum Information, Forschungszentrum Jülich and RWTH Aachen, 52074 Aachen, Germany
- Anja Zass Peter Grünberg Institute 10 (PGI 10), Forschungszentrum Jülich, 52428 Jülich, Germany
- Lars R. Schreiber JARA-FIT Institute for Quantum Information, Forschungszentrum Jülich and RWTH Aachen, 52074 Aachen, Germany
- Alexander Pawlis Peter Grünberg Institute 9 (PGI 9), Forschungszentrum Jülich, 52428 Jülich, Germany; Peter Grünberg Institute 10 (PGI 10), Forschungszentrum Jülich, 52428 Jülich, Germany; JARA-Fundamentals of Future Information Technology (JARA-FIT), 52428 Jülich, Germany; orcid.org/0000-0002-3394-0707

Complete contact information is available at: https://pubs.acs.org/10.1021/acsaelm.4c01104

Author Contributions

N.v.d.D., L.R.S., and A.P. designed the experiments. Y.K. and F.K. fabricated the shadow wall templates. N.v.d.D. performed epitaxial growth and X-ray characterization. N.v.d.D. and Y.K. conducted PL spectroscopy measurements. A.Z. conducted AFM investigations. N.v.d.D, Y.K., F.K., L.R.S., and A.P. wrote the manuscript. All authors have given approval to the final version of the manuscript.

Notes

The authors declare no competing financial interest.

ACKNOWLEDGMENTS

We gratefully acknowledge the technical support and service by C. Krause, B. Bennemann, T. Brazda, and C. Falter and from the staff of the Helmholtz Nano Facility (HNF). We further gratefully acknowledge technical support by J. Ehrler, J. Gruis, and A. Vescan in early generations of shadow walls. This work is supported by the German Research Foundation (DFG) within the project no. 337456818 and under Germany's Excellence Strategy framework within the Cluster of Excellence Matter and Light for Quantum Computing (ML4Q) (EXC 2004/1-390534769).

■ REFERENCES

- (1) Ren, J.; Bowers, K. A.; Sneed, B.; Dreifus, D. L.; Cook, J. W.; Schetzina, J. F.; Kolbas, R. M. ZnSe light-emitting diodes. *Appl. Phys. Lett.* **1990**, *57*, 1901–1903.
- (2) Haase, M. A.; Qiu, J.; DePuydt, J. M.; Cheng, H. Blue-green laser diodes. *Appl. Phys. Lett.* **1991**, *59*, 1272–1274.
- (3) Katayama, K.; Matsubara, H.; Nakanishi, F.; Nakamura, T.; Doi, H.; Saegusa, A.; Mitsui, T.; Matsuoka, T.; Irikura, M.; Takebe, T.; Nishine, S.; Shirakawa, T. ZnSe-based white LEDs. *J. Cryst. Growth* **2000**, 214–215, 1064–1070.
- (4) Sun, Q.; Wang, Y. A.; Li, L. S.; Wang, D.; Zhu, T.; Xu, J.; Yang, C.; Li, Y. Bright, multicoloured light-emitting diodes based on quantum dots. *Nat. Photonics* **2007**, *1*, 717–722.
- (5) Ladd, T. D.; Sanaka, K.; Yamamoto, Y.; Pawlis, A.; Lischka, K. Fluorine-doped ZnSe for applications basic solid state physics in quantum information processing. *Physica Status Solidi* (B) Basic Research 2010, 247, 1543–1546.

- (6) Kutovyi, Y.; Jansen, M. M.; Qiao, S.; Falter, C.; von den Driesch, N.; Brazda, T.; Demarina, N.; Trellenkamp, S.; Bennemann, B.; Grützmacher, D.; Pawlis, A. Efficient Single-Photon Sources Based on Chlorine-Doped ZnSe Nanopillars with Growth Controlled Emission Energy. *ACS Nano* **2022**, *16*, 14582–14589.
- (7) Tribu, A.; Sallen, G.; Aichele, T.; André, R.; Poizat, J. P.; Bougerol, C.; Tatarenko, S.; Kheng, K. A high-temperature single-photon source from nanowire quantum dots. *Nano Lett.* **2008**, 8, 4326–4329.
- (8) Karasahin, A.; Pettit, R. M.; von den Driesch, N.; Jansen, M. M.; Pawlis, A.; Waks, E. Single quantum emitters with spin ground states based on Cl bound excitons in ZnSe. *Phys. Rev. A* **2022**, *106*, 1030402
- (9) Sleiter, D. J.; Sanaka, K.; Kim, Y. M.; Lischka, K.; Pawlis, A.; Yamamoto, Y. Optical Pumping of a Single Electron Spin Bound to a Fluorine Donor in a ZnSe Nanostructure. *Nano Lett.* **2013**, *13*, 116–120
- (10) Sanaka, K.; Pawlis, A.; Ladd, T. D.; Sleiter, D. J.; Lischka, K.; Yamamoto, Y. Entangling Single Photons from Independently Tuned Semiconductor Nanoemitters. *Nano Lett.* **2012**, *12*, 4611–4616.
- (11) Pawlis, A.; Mussler, G.; Krause, C.; Bennemann, B.; Breuer, U.; Grützmacher, D. MBE Growth and Optical Properties of Isotopically Purified ZnSe Heterostructures. *ACS Applied Electronic Materials* **2019**, *1*, 44–50.
- (12) Kirstein, E.; Zhukov, E. A.; Smirnov, D. S.; Nedelea, V.; Greve, P.; Kalitukha, I. V.; Sapega, V. F.; Pawlis, A.; Yakovlev, D. R.; Bayer, M.; Greilich, A. Extended spin coherence of the zinc-vacancy centers in ZnSe with fast optical access. *Communications Materials* **2021**, *2*, 91
- (13) Janßen, J.; Hartz, F.; Huckemann, T.; Kamphausen, C.; Neul, M.; Schreiber, L. R.; Pawlis, A. Low-Temperature Ohmic Contacts to n-ZnSe for all-Electrical Quantum Devices. *ACS Applied Electronic Materials* **2020**, *2*, 898–905.
- (14) Burkard, G.; Ladd, T. D.; Pan, A.; Nichol, J. M.; Petta, J. R. Semiconductor spin qubits. *Rev. Mod. Phys.* **2023**, *95*, 025003.
- (15) Vandersypen, L. M. K.; Bluhm, H.; Clarke, J. S.; Dzurak, A. S.; Ishihara, R.; Morello, A.; Reilly, D. J.; Schreiber, L. R.; Veldhorst, M. Interfacing spin qubits in quantum dots and donors—hot, dense, and coherent. *npj Quantum Information* **2017**, *3*, 34.
- (16) Hanson, R.; Kouwenhoven, L. P.; Petta, J. R.; Tarucha, S.; Vandersypen, L. M. K. Spins in few-electron quantum dots. *Rev. Mod. Phys.* **2007**, *79*, 1217–1265.
- (17) Scappucci, G.; Kloeffel, C.; Zwanenburg, F. A.; Loss, D.; Myronov, M.; Zhang, J. J.; De Franceschi, S.; Katsaros, G.; Veldhorst, M. The germanium quantum information route. *Nature Reviews Materials* **2021**, *6*, 926–943.
- (18) Neul, M.; Sprave, I. V.; Diebel, L. K.; Zinkl, L. G.; Fuchs, F.; Yamamoto, Y.; Vedder, C.; Bougeard, D.; Schreiber, L. R. Local laser-induced solid-phase recrystallization of phosphorus-implanted Si/SiGe heterostructures for contacts below 4.2 K. *Physical Review Materials* **2024**, *8*, 043801.
- (19) Losert, M. P.; Eriksson, M. A.; Joynt, R.; Rahman, R.; Scappucci, G.; Coppersmith, S. N.; Friesen, M. Practical strategies for enhancing the valley splitting in Si/SiGe quantum wells. *Phys. Rev. B* **2023**, *108*, 125405.
- (20) Volmer, M.; Struck, T.; Sala, A.; Chen, B.; Oberländer, M.; Offermann, T.; Xue, R.; Visser, L.; Tu, J.-S.; Trellenkamp, S.; Cywiński, Ł.; Bluhm, H.; Schreiber, L. R. Mapping of valley splitting by conveyor-mode spin-coherent electron shuttling. *npj Quantum Information* **2024**, *10*, 61.
- (21) Passow, T.; Leonardi, K.; Heinke, H.; Hommel, D.; Litvinov, D.; Rosenauer, A.; Gerthsen, D.; Seufert, J.; Bacher, G.; Forchel, A. Quantum dot formation by segregation enhanced CdSe reorganization. *J. Appl. Phys.* **2002**, *92*, 6546–6552.
- (22) Gunshor, R.; Kolodziejski, L. Recent advances in the molecular beam epitaxy of the wide-bandgap semiconductor ZnSe and its superlattices. *IEEE J. Quantum Electron.* **1988**, 24, 1744–1757.

- (23) Singh, D. K.; Gupta, G. van der Waals epitaxy of transition metal dichalcogenides via molecular beam epitaxy: looking back and moving forward. *Materials Advances* **2022**, *3*, 6142–6156.
- (24) Schüffelgen, P.; Rosenbach, D.; Li, C.; Schmitt, T. W.; Schleenvoigt, M.; Jalil, A. R.; Schmitt, S.; Kölzer, J.; Wang, M.; Bennemann, B.; Parlak, U.; Kibkalo, L.; Trellenkamp, S.; Grap, T.; Meertens, D.; Luysberg, M.; Mussler, G.; Berenschot, E.; Tas, N.; Golubov, A. A.; Brinkman, A.; SchäPers, T.; Grützmacher, D. Selective area growth and stencil lithography for in situ fabricated quantum devices. *Nat. Nanotechnol.* **2019**, *14*, 825–831.
- (25) Wu, X.; Gulden, K. H.; Thomas, M.; Wilson, G.; Walker, J.; Döhler, G. H.; Whinnery, J. R.; Smith, J. S. Selectively masked MBE regrowth. *J. Cryst. Growth* 1993, 127, 896–899.
- (26) Goldstein, L.; Glas, F.; Marzin, J. Y.; Charasse, M. N.; Le Roux, G. Growth by molecular beam epitaxy and characterization of InAs/GaAs strained-layer superlattices. *Appl. Phys. Lett.* **1985**, 47, 1099–1101.
- (27) Lee, J. H.; Wang, Z. M.; Kim, E. S.; Kim, N. Y.; Park, S. H.; Salamo, G. J. Various Quantum- and Nano-Structures by III–V Droplet Epitaxy on GaAs Substrates. *Nanoscale Res. Lett.* **2010**, *5*, 308.
- (28) Schallenberg, T.; Schumacher, C.; Faschinger, W. In situ structuring during MBE regrowth with shadow masks. *Physica E: Low-dimensional Systems and Nanostructures* **2002**, *13*, 1212–1215.
- (29) Schallenberg, T.; Molenkamp, L. W.; Karczewski, G. Molecular beam epitaxy of compound materials through shadow masks. *Phys. Rev. B* **2004**, *70*, 155328.
- (30) Schumacher, C.; Faschinger, W. Self-organized nucleation of sharply defined nanostructures during growth into shadow masks. *J. Cryst. Growth* **2000**, 214–215, 732–736.
- (31) Heedt, S.; Quintero-Pérez, M.; Borsoi, F.; Fursina, A.; van Loo, N.; Mazur, G. P.; Nowak, M. P.; Ammerlaan, M.; Li, K.; Korneychuk, S.; Shen, J.; van de Poll, M. A. Y.; Badawy, G.; Gazibegovic, S.; de Jong, N.; Aseev, P.; van Hoogdalem, K.; Bakkers, E. P. A. M.; Kouwenhoven, L. P. Shadow-wall lithography of ballistic superconductor—semiconductor quantum devices. *Nat. Commun.* **2021**, *12*, 4914.
- (32) Jiang, Y.; Yang, S.; Li, L.; Song, W.; Miao, W.; Tong, B.; Geng, Z.; Gao, Y.; Li, R.; Chen, F.; Zhang, Q.; Meng, F.; Gu, L.; Zhu, K.; Zang, Y.; Shang, R.; Cao, Z.; Feng, X.; Xue, Q. K.; Liu, D. E.; Zhang, H.; He, K. Selective area epitaxy of PbTe-Pb hybrid nanowires on a lattice-matched substrate. *Physical Review Materials* **2022**, *6*, 034205.
- (33) Zhang, C.; Alberi, K.; Honsberg, C.; Park, K. Investigation of GaAs surface treatments for ZnSe growth by molecular beam epitaxy without a buffer layer. *Appl. Surf. Sci.* **2021**, *549*, 149245.
- (34) Riley, J.; Wolfframm, D.; Westwood, D.; Evans, A. Studies in the growth of ZnSe on GaAs(001). *J. Cryst. Growth* **1996**, *160*, 193–200.
- (35) Schallenberg, T.; Schumacher, C.; Molenkamp, L. W. Projective techniques for the growth of compound semiconductor nanostructures. *Physica Status Solidi* (A) Applied Research 2003, 195, 232–237.
- (36) Horsburgh, G.; Prior, K. A.; Meredith, W.; Galbraith, I.; Cavenett, B. C.; Whitehouse, C. R.; Lacey, G.; Cullis, A. G.; Parbrook, P. J.; Möck, P.; Mizuno, K. Topography measurements of the critical thickness of ZnSe grown on GaAs. *Appl. Phys. Lett.* **1998**, 72, 3148–3150
- (37) Park, K.; Alberi, K. A strategy to eliminate selenium oxide islands formed on the ZnSe/GaAs epilayer. *Materials Science in Semiconductor Processing* **2024**, *174*, 108176.
- (38) Gutowski, J.; Presser, N.; Kudlek, G. Optical Properties of ZnSe Epilayers and Films. *Physica Status Solidi* (a) **1990**, 120, 11–59.
- (39) Pawlis, A.; Berstermann, T.; Brüggemann, C.; Bombeck, M.; Dunker, D.; Yakovlev, D. R.; Gippius, N. A.; Lischka, K.; Bayer, M. Exciton states in shallow ZnSe/(Zn,Mg)Se quantum wells: Interaction of confined and continuum electron and hole states. *Phys. Rev. B* **2011**, 83, 115302.